Dirac fermions in graphene using the position-dependent translation operator formalism

V. Aguiar, S. M. Cunha, D. R. da Costa,* and Raimundo N. Costa Filho †
Departamento de Física, Universidade Federal do Ceará, Campus do Pici, 60455-760 Fortaleza, Ceará, Brazil

(Received 10 September 2020; revised 31 October 2020; accepted 9 November 2020; published 3 December 2020)

Within the position-dependent translation operator formalism for quantum systems, we obtain analytical expressions for the eigenstates and the Landau level spectrum of Dirac fermions in graphene in the presence of a perpendicularly applied magnetic field and, as a consequence of the formalism, with a generalized form of the momentum operator. Moreover, we explore the behavior of wave packet dynamics in such a system by considering different initial pseudospin polarizations and metric parameters. Our findings show that the Landau levels, the wave packet trajectories, and velocities are significantly affected by the choice of the metric in the non-Euclidean space of the deformed momentum operator, exhibiting a tunable energy level spacing. In the dynamics analysis, one observes an enhancement of the oscillation amplitude of the average positions for all investigated pseudospin polarizations due to the nonsymmetric evolution of the wave packet induced by the different metrics in the system. The present formalism is shown to be a theoretical platform to describe the effects of two scenarios due to (i) a lattice deformation in graphene, giving rise to a natural Fermi velocity renormalization, or even (ii) a nonuniform mass term, induced by a specific substrate, that varies on a length scale much greater than the magnetic field length.

DOI: 10.1103/PhysRevB.102.235404

I. INTRODUCTION

During the past two decades, many studies have been carried out to understand the unique properties of graphene, a single atomic thin layer of graphite [1,2]. A plethora of its exotic features, such as the Klein tunneling effect and unusual quantum Hall effect, originate from the fact that low-energy charge carriers in graphene obey the zero-mass Dirac equation, providing a favorable environment to probe interesting phenomena predicted by quantum field theories not found in conventional semiconductors and metals. One consequence of its gapless linear dispersion, in the presence of a perpendicular magnetic field, is the $\sqrt{B}$ dependence on the Landau levels in contrast to the linear dependence on B observed in a conventional two-dimensional (2D) electron gas spectrum for Schrödinger fermions [3–6].

Another very interesting property of massless Dirac fermions in graphene is that they experience Zitterbewegung, a trembling motion caused by interference between positive and negative energy states [7,8] that was predicted by Schrödinger for the motion of relativistic electrons in vacuum governed by the Dirac equation. Therefore, stimulated by Schrödinger's idea, numerous theoretical works have investigated the dynamics of wave packets in a 2D electron gas [7–12] and, more recently, in 2D materials, for example, single-layer [13–22] and bilayer [13,17,23] graphene, silicene [24], transition metal dichalcogenides [25], and multilayer phosphorene [26].

From the theoretical point of view in the analysis of quantum systems, in recent years there has been a growing body of literature dealing with systems consisting of particles with position-dependent mass [27–43]. Most of the previous approaches [27–39] considered a modification of canonical commutation relations or even modifications in the underlying space, which leads to the problem of ordering in the kinetic energy operator since in this formalism mass is mapped onto an operator that does not commute with the momentum operator [44]. To overcome this issue, Costa Filho *et al.* [40] in 2011 proposed a new method that consists of a generalized translation operator which produces infinitesimal spatial displacements, such that $T(dx)|x\rangle = |x + g_{xx}^{-1/2}dx\rangle$, where $g_{xx}^{-1/2}$ is a function of the position and related to the metric. It changes the momentum and, consequently, the commutation relation between momentum and position into a more generalized form and leads to a modified Schrödinger equation that resembles the standard Schrödinger equation to describe charge carriers with position-dependent effective masses. Thereafter, a series of recent studies have used this position-dependent translation operator formalism [40–43,45–49].

Based on the Costa Filho formalism [40–43] and motivated by the great interest in 2D materials due to their colossal possible future technological applications, in this work we extend the previous reported analysis for the case of graphene in the presence of a perpendicular magnetic field, and we show that the metric in this formalism can be viewed as an additional mechanism for controlling the electronic and transport properties of low-energy electrons in graphene; we also discuss it in view of two scenarios due to the lattice deformation and to a position-dependent mass term induced by a specific substrate. To perform this investigation, we analytically solve the Dirac equation with a generalized momentum operator and discuss the role of the metric in the eigenstates and energy spectrum. Moreover, we time evolve a Gaussian wave packet, describing charge carriers traveling through the system, and calculate

*diego_rabelo@fisica.ufc.br
†rai@fisica.ufc.br

the expectation values of the position operator and velocity operator as a function of time, discussing the main features of the Zitterbewegung effect for different initial pseudospin polarizations and metrics.

The present paper is organized as follows. In Sec. II we present the theoretical framework used in this paper, showing the analytical solution of the Dirac equation for monolayer graphene in the presence of a perpendicularly applied magnetic field and with a deformed momentum along the x direction due to a general metric originating from the position-dependent translation operator formalism. The results of the analytically calculated Landau levels for a generic metric are also shown and compared with the nondeformed case. In Sec. III, we investigate the wave packet dynamics and how some physical quantities, such as average positions and average velocities, evolve in time for the studied graphene system with a generic metric. Results for different metrics, for different initial pseudospin polarizations, and for the manifestation of the Zitterbwegung on the wave packet motion in graphene with this deformed metric are discussed. A summary and concluding remarks are reported in Sec. IV.

II. ELECTRONIC PROPERTIES OF GRAPHENE WITH A GENERIC METRIC

The energy spectrum of an infinite undoped graphene sheet in the presence of a magnetic field and in the vicinity of the Dirac cones can be obtained by solving the eigenvalue equation $H_D\Psi(x,y) = E\Psi(x,y)$ with the following Dirac-Weyl Hamiltonian [50,51]:

$$H_D = v_F\vec{\sigma}\cdot(\vec{\mathcal{P}} + e\vec{A}) + \tau\Delta\sigma_z, \tag{1}$$

where v_F is the Fermi velocity, e is the electron charge, $\vec{A}$ is the electromagnetic vector potential, $\vec{\sigma} = (\sigma_x, \sigma_y, \sigma_z)$ denotes the Pauli matrix, Δ $(-\Delta)$ is the on-site potential induced by the substrate on the A (B) sublattice, which can be seen as a mass term within the continuum model, and τ is the valley index, being 1 (-1) for the K (K') Dirac point. Based on the position-dependent translation operator formalism [40–43], the generalized position-dependent momentum operator associated with a spatial displacement that generates the translation from point ν to $\nu + g_{\nu\nu}^{-1/2}d\nu$ can be written as $\mathcal{P}_\nu = -i\hbar g_{\nu\nu}^{-1/2}\frac{\partial}{\partial\nu}$, with $\nu = x$, y, and z, where $g_{\nu\nu}^{-1/2}$ is a function of the position and related to the metric. In fact, $g_{\nu\nu}^{-1/2}$ is an element of a diagonal metric of the non-Euclidean space under consideration. The eigenstates of the Hamiltonian (1) are the two-component spinors $\Psi = [\Psi_A, \Psi_B]^T$, where Ψ_A (Ψ_B) are the envelope functions associated with the probability amplitudes of sublattice A (B).

For convenience, we choose the Landau gauge $\vec{A} = (0, B_0x, 0)$, such that the system has translational invariance only along the y direction (i.e., $\mathcal{P}_y = \hbar k_y$). Thus, one can assume solutions such as the following ansatz:

$$\Psi(x,y) = e^{ik_y\int g_{yy}^{1/2}dy}\begin{pmatrix}\psi_+(x)\\ \psi_-(x)\end{pmatrix}. \tag{2}$$

With the Hamiltonian (1) acting on the two-component wave function (2), one obtains the following set of coupled differential equations:

$$\left[\frac{1}{\sqrt{g_{xx}}}\frac{d}{dx} + \frac{(x-x_0)}{l_B^2}\right]\psi_- = i\frac{(E-\tau\Delta)}{\hbar v_F}\psi_+, \tag{3a}$$

$$\left[\frac{1}{\sqrt{g_{xx}}}\frac{d}{dx} - \frac{(x-x_0)}{l_B^2}\right]\psi_+ = i\frac{(E+\tau\Delta)}{\hbar v_F}\psi_-, \tag{3b}$$

where $x_0 = -\frac{\hbar k_y}{eB_0} = -l_B^2k_y$ and $l_B = \sqrt{\frac{\hbar}{eB_0}}$ is the magnetic length.

Decoupling the above set of equations (3) with respect to ψ_+, we arrive at

$$\frac{d^2\psi_+(\eta)}{d\eta^2} + \left[\frac{(E^2-\Delta^2)}{\hbar^2v_F^2} - \frac{e^{\sqrt{g}\frac{\eta}{l_B}}}{l_B^2} - \frac{(e^{\sqrt{g}\frac{\eta}{l_B}}-1)^2}{gl_B^2}\right]\psi_+(\eta) = 0, \tag{4}$$

where we consider the spatial metric as the linear function,

$$g_{xx}^{-1/2} = 1 + \frac{\sqrt{g}}{l_B}(x-x_0), \tag{5}$$

and the application of the transformation

$$\eta(x) = \int g_{xx}^{1/2}dx = \frac{l_B}{\sqrt{g}}\ln\left[1 + \frac{\sqrt{g}}{l_B}(x-x_0)\right] \tag{6}$$

in order to eliminate the first derivative in Eq. (4). Notice that g is a dimensionless parameter that is associated with the effect of space modification. It is easy to note that for $g = 0$ we recover the nonmodified Dirac equation with the metric equal to 1 (i.e., $\mathcal{P}_\nu \to -i\hbar\frac{\partial}{\partial\nu}$). Therefore, the appropriate length scale for the problem is the magnetic length l_B. To illustrate this spatial deformation on the η axis, Fig. 1 depicts dependence of η as a function of the real and nondeformed x coordinate [Eq. (6)] in the case of a linear metric as given by Eq. (5). Three different metric parameters g were assumed, and magnetic field amplitude was fixed at $B = 1$ T. We can realize from Fig. 1 that the introduction of a non-null metric parameter g induces a deformation in the η space, such that η is moving away from a linear relation with respect to the x coordinate to higher values of g, as can be seen by comparing

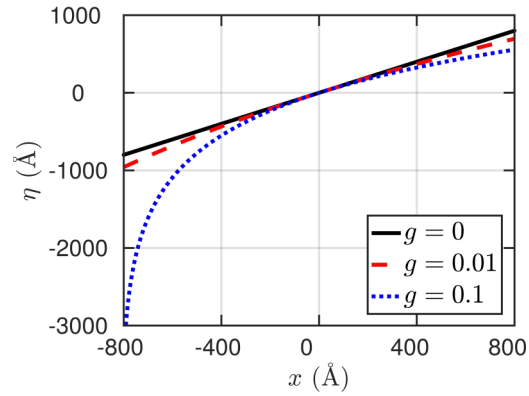

FIG. 1. Deformed η coordinate as a function of the nondeformed x coordinate in real space [see Eq. (6)] for three different metric parameters: black solid line, $g = 0$; red dashed line, $g = 0.01$; and blue dotted line, $g = 0.1$. A magnetic field amplitude of $B = 1$ T was assumed.

the cases $g = 0$ and $g = 0.1$, and $\eta < 0$ is the most affected direction.

From Eq. (4), we can obtain the wave functions ψ_+ and ψ_-, given, respectively, by

$$\psi_+(\eta) = A_n \beta^s e^{-\beta} L_n^{2s}(2\beta), \tag{7a}$$

$$\psi_-(\eta) = \frac{A_n \beta^s e^{-\beta} i\hbar v_F}{l_B\sqrt{g}(E+\tau\Delta)} \times \left\{2e^{\frac{\sqrt{g}\eta}{l_B}} L_{n-1}^{2s+1}(2\beta) + [2e^{\frac{\sqrt{g}\eta}{l_B}} - (1+gs)]L_n^{2s}(2\beta)\right\}, \tag{7b}$$

where $\beta = \frac{1}{g}e^{\sqrt{g}\eta/l_B}$, $s = \frac{1}{g} - (n+1)$, L_n^{2s} is the generalized Laguerre polynomial, and A_n is the normalization constant. The corresponding energy levels read

$$E_n = \pm\hbar v_F \sqrt{\frac{\Delta^2}{\hbar^2 v_F^2} + \frac{2}{l_B^2}(n+1) - \frac{g}{l_B^2}(n+1)^2}, \tag{8}$$

with $n \in \mathcal{N}$. The positive values correspond to electrons (conduction band), while the negative values correspond to holes (valence band). Repeating the same decoupling procedure of the set of equations (3) but now for the ψ_- component, we find

$$E_n = \pm\hbar v_F \sqrt{\frac{\Delta^2}{\hbar^2 v_F^2} + \frac{n(2-gn)}{l_B^2}}. \tag{9}$$

By taking $g = 0$ in Eqs. (8) and (9), we can easily obtain the Landau level energies for the nondeformed graphene which depends on the square root of both the level index n and the magnetic field B and exhibits a different dependence on the energy levels for sublattices A [$E_n \propto \sqrt{2(n+1)}$] and B ($E_n \propto \sqrt{2n}$). It is in contrast to the standard 2D electron gas, whose Landau levels are equally spaced. Notice that for the graphene case with $g \neq 0$, we have an additional contribution term for the Landau levels that is proportional to the metric g and has an n^2 dependence. It is easy to realize from Eqs. (8) and (9) that there is a range of valid g values to obtain real energy levels, given by $g \leqslant (\frac{\Delta l_B}{\hbar v_F n'})^2 + \frac{2}{n'}$, with $n' = 0, 1, 2, \ldots$; that is, for a fixed g parameter only some n' values are allowed. As we shall discuss further, this term is responsible for changing the charge carrier electronic properties in graphene with a generic metric when compared to the nondeformed case, and also it causes a shift in the energy spectrum. For $\Delta = 0$, note that Eq. (8) lacks the level with $E = 0$ that is present in Eq. (9), and the introduction of a different metric does not lift the degeneracy of the twofold zeroth Landau levels since $E_0 = 0$ from Eq. (9), unlike the mass term Δ that opens a gap of 2Δ in the spectrum, and in addition the presence of Δ shifts the Landau level spectrum for $n \neq 0$. The existence of a zeroth Landau level $E_0 = 0$ is a direct consequence of the zero gap in the energy spectrum for Dirac fermions in graphene and is due to its chiral symmetry [52]. An important remark about Eqs. (8) and (9) is that the Landau levels are independent of the valley index, and therefore, the Landau level for $n \neq 0$ ($n = 0$) has fourfold (twofold) degeneracy, being twofold associated with the electron-hole symmetry and twofold associated with valley symmetry [4–6].

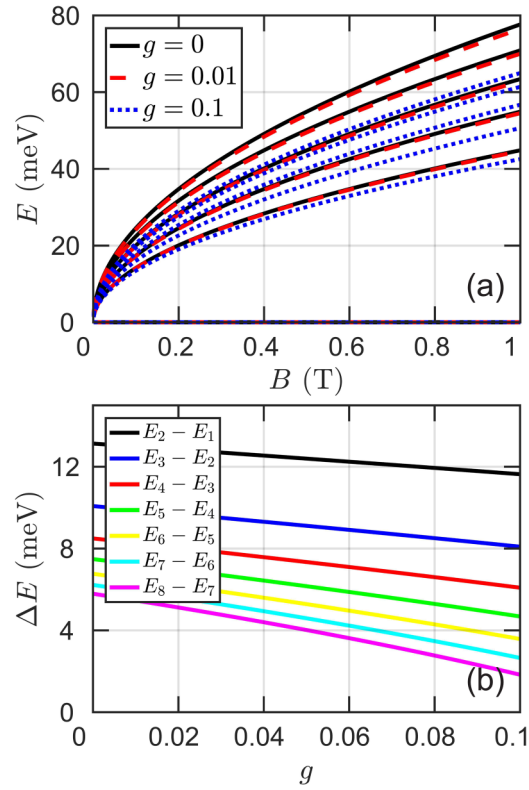

FIG. 2. (a) The lowest five Landau levels for electrons as a function of perpendicular magnetic field for metrics $g = 0$ (solid black lines), $g = 0.01$ (dashed red lines), and $g = 0.1$ (dotted blue lines). (b) Energy level spacing between two adjacent states $E_{n+1} - E_n$ as a function of the metric for a fixed magnetic field amplitude $B = 1$ T and a null mass term $\Delta = 0$.

The dependence of the lowest-energy levels on the magnetic field for the unbiased graphene system for $g = 0$ (solid black lines) and for $g \neq 0$ (dashed red lines for $g = 0.01$ and dotted blue lines for $g = 0.1$) is shown in Fig. 2(a). A consequence of the metric change is a shift in the energy levels, together with a change in level spacing, as emphasized in Fig. 2(b), which depicts the behavior of the level spacing as a function of the metric g, fixing magnetic field amplitude $B = 1$ T. It is seen that as the metric increases, the energy levels are shifted to lower values, and the spacing between them decreases too, which in turn increases the number of accessible electronic states for a fixed energy range. Note that these behaviors of the deformed Landau levels with respect to the metric resemble those observed in the following two scenarios: (i) strained graphene, such that both the lattice and Dirac cones are distorted, which leads to a spatial dependence and anisotropy of the Fermi velocity induced by the lattice change through a renormalized linear momentum [53–57], and (ii) a single-layer graphene sheet deposited on a specific deformed substrate, such that the substrate-induced mass term is nonuniform and varies on a length scale much greater than the magnetic field length [58]. In both scenarios, the Landau levels change qualitatively in a similar way, as shown in Fig. 2(a), i.e., exhibiting a contraction effect of the Landau levels spectra. With respect to the first scenario, it is worth mentioning that a more direct analogy with the considered

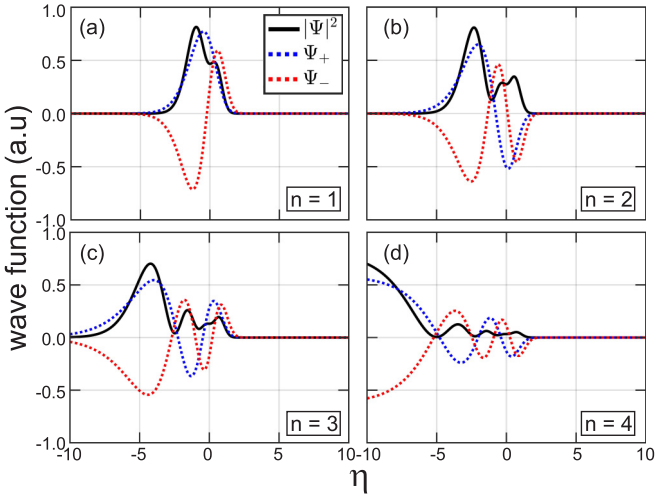

FIG. 3. The wave function amplitude for the first four excited levels, (a) $n = 1$, (b) $n = 2$, (c) $n = 3$, and (d) $n = 4$. The black solid, blue dashed, and red dashed lines correspond to the total wave function and the two pseudospin components ψ_+ and ψ_-, respectively. The metric is $g = 0.25$, and the assumed magnetic field is $B = 1$ T. $\Im\{\psi_-\}$ is shown since it is purely imaginary. The unit of η is angstroms.

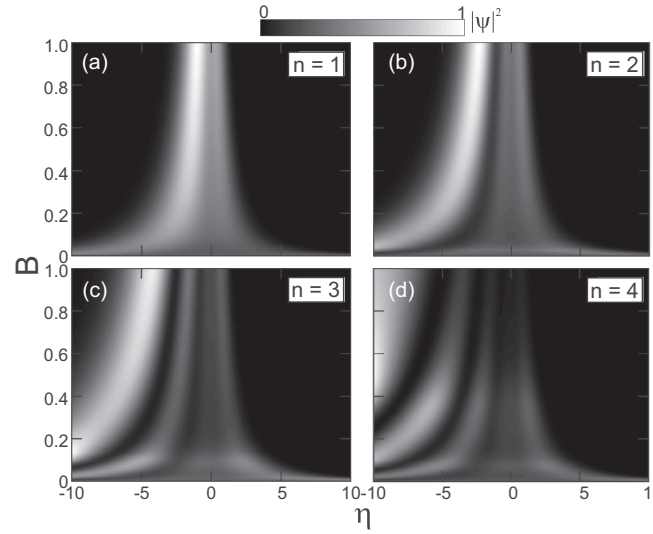

FIG. 4. The dependence of the wave function on the magnetic field for the metric $g = 0.25$ and for the first four excited levels: (a) $n = 1$, (b) $n = 2$, (c) $n = 3$, and (d) $n = 4$. The amplitude increases from black to white. The units of the magnetic field amplitude and η are teslas and angstroms, respectively.

position-dependent spatial metric given by the linear function Eq. (5) is uniaxially strained graphene. In this context, a recent work [53] described such unidirectional deformation by using renormalized linear momentum in an effective Dirac-like Hamiltonian that, similar to the current work, can capture the feature of the contraction of the Landau levels, but as a function of the deformation amplitude, instead of the metric as treated here. In both cases, owing to the strain or metric change, the contraction of the Landau level energies can be understood by the renormalization of the Fermi velocity. From this point of view, one can get an explicit relation showing quantitatively direct correspondence between the spatial metric g and the different types of strain in graphene, such that it is possible to find $g \equiv g(\epsilon)$, with ϵ being the amplitude of the lattice deformation.

From the analytical expressions (7a) and (7b), we plot in Fig. 3 the four first excited wave functions for the graphene case with a non-null metric assumed to be $g = 0.25$ and a fixed magnetic field amplitude $B = 1$ T. The solid black, dashed blue, and dashed red lines correspond to the total wave function $|\Psi|^2$ and the two pseudopsin components ψ_+ and ψ_-, respectively. For the nondeformed graphene case, it is well known [4–6,59] that solutions in the presence of an external magnetic field are given by the Hermitian polynomials and $|\Psi|^2$ is symmetric with respect to $\eta = 0$. Note that the total wave function and the two components of the pseudospinor are no longer spatially symmetric when we assume a non-null parameter g. In analogy with strained graphene, such a lack of spatial symmetry of the wave functions can be understood by the lattice deformation in graphene that causes in the microscopic point of view changes in the interatomic distances and in the hopping energies of the carbon atoms and, consequently, a modification in the electronic band structure. Such distortions on the Dirac cones can lead to an anisotropic position-dependent Fermi velocity which, in turn, can be seen as an anisotropy and a position dependence on the effective masses of the system. Therefore, within this analogy, the wave function is more (less) localized at the regions where the kinetic energy is lowest (highest) due to the highest (lowest) effective mass along a certain direction. Note from Fig. 3 that due to the non-null metric, the wave functions with higher energetic states exhibit a strong localization for $\eta < 0$ that can be associated with the region with higher effective mass, lower renormalized Fermi velocity, and the most affected η direction, as demonstrated in Fig. 1. Similar results for deformed graphene systems were already reported in the literature such as strong localization along the deformed direction [53–57]. A very interesting aspect of the spatial distribution of the two-component wave functions is that, even for the non-deformed case ($g = 0$), the occupation of the sublattices displays a natural asymmetric occupation which originates from asymmetry in positions of the nearest neighbors for atoms in the A and B sublattices due to the different dependences of the energy levels for sublattices A [Eq. (8)] and B [Eq. (9)], which differ in the index n from 1. Moreover, Eq. (4) resembles a differential equation of a particle subjected to an effective Morse-type potential [43] in η space, i.e., $[d^2/d\eta^2 + V_{\text{eff}}(\eta)]\psi_+ = E'\psi_+$, which is the effective potential of the term inside the brackets in Eq. (4) without the energy term $E' = (E/\hbar v_F)^2$. Note also that Fig. 3 shows strong asymmetry in the probability density, which implies that it is more probable to find the particle in the regions of maximum potential. In Refs. [60,61], the authors showed that such asymmetry can be obtained when a particle is subjected to an exponential-type magnetic field. However, in the current work we obtain similar results by applying a constant magnetic field in $\{x, y\}$ space.

In addition to the wave function analysis for a graphene system with a generic metric, Figs. 4(a)–4(d) show contour plots of the first ($n = 1$), second ($n = 2$), third ($n = 3$), and

fourth ($n = 4$) excited total wave functions, respectively, by varying the magnetic field amplitude but keeping a fixed value of the metric of $g = 0.25$. As already expected, as the magnetic field increases, the magnetic length decreases, and consequently, the wave functions become more confined. Hence, although the introduction of a different metric (i.e., $g \neq 0$) delocalizes the wave function, giving rise to spatial asymmetry, the effect of strong magnetic fields is able to overcome such delocalization.

III. WAVE PACKET DYNAMICS IN GRAPHENE WITH A GENERIC METRIC

Let us now investigate the effect on the wave packet dynamics in the presence of external magnetic field due to a nonunitary metric [i.e., for $g_{\nu\nu} \neq 1$ or, equivalently, for $g \neq 0$ in Eq. (5)], owing to a generalized position-dependent momentum operator in the considered formalism, and we shall also discuss the results of the role of a different metric in association with different physical scenarios already reported in the literature [53–56,58] and also discussed in Sec. II. In this analysis, we explore the time-dependent average positions and velocities and the snapshots in real space of the wave packet evolution by taking different metric parameters g and different initial pseudospin polarizations. To do this, we use the well-known split-operator technique [26,62–75] for wave packet propagation in real time that consists of the solution of the time-dependent Schrödinger equation $i\hbar\partial\Psi(\vec{r},t) = H\Psi(\vec{r},t)$ by taking a separation of the time-evolution operator $\hat{U} = \exp[-iH\Delta t/\hbar]$ in a series of matrices, such that the propagated wave function after a time step Δt can be calculated by applying the expanded exponential time-evolution operator to the wave packet at any instant t, i.e., $\Psi(\vec{r}, t + \Delta t) = \hat{U}\Psi(\vec{r}, t)$.

Like in Sec. II, to calculate the quantum electronic trajectories using a wave packet within the split-operator technique, we consider (i) the continuum model Hamiltonian H_D given by Eq. (1) for the description of low-energy massless fermions, (ii) the deformed momentum along the x direction given by $\mathcal{P}_x = -i\hbar g_{xx}^{-1/2}\frac{\partial}{\partial_x}$, and (iii) the linear function for the metric given by Eq. (5). The initial wave packet is assumed to be a circularly symmetric Gaussian distribution, multiplied by a pseudospinor $[c_1, c_2]^T$ that accounts for the probability distributions over the two sublattices of graphene (labeled A and B) and by a plane wave with wave vector $\vec{k} = (k_x, k_y)$, which gives the wave packet a nonzero average momentum, defined as

$$\Psi(\vec{r},0) = N\begin{pmatrix} c_1 \\ c_2 \end{pmatrix}\exp\left[-\frac{(x-x_0)^2+(y-y_0)^2}{d^2} + i(\vec{k}\cdot\vec{r})\right], \tag{10}$$

where N is a normalization factor, (x_0, y_0) are the coordinates of the center of the Gaussian wave packet, and d is its width. For our study, the initial position of the wave packet is at $(x_0, y_0) = (0, 0)$; its width is assumed to be $d = l_B$, with $l_B = \sqrt{\hbar/eB_0}$ corresponding to the magnetic length for a fixed magnetic field amplitude considered to be $B_0 = 10$ T (and thus $l_B = 81.13$ Å), and its initial momentum is $(k_x^0, k_y^0) = (0.035, 0)$ Å^{-1}.

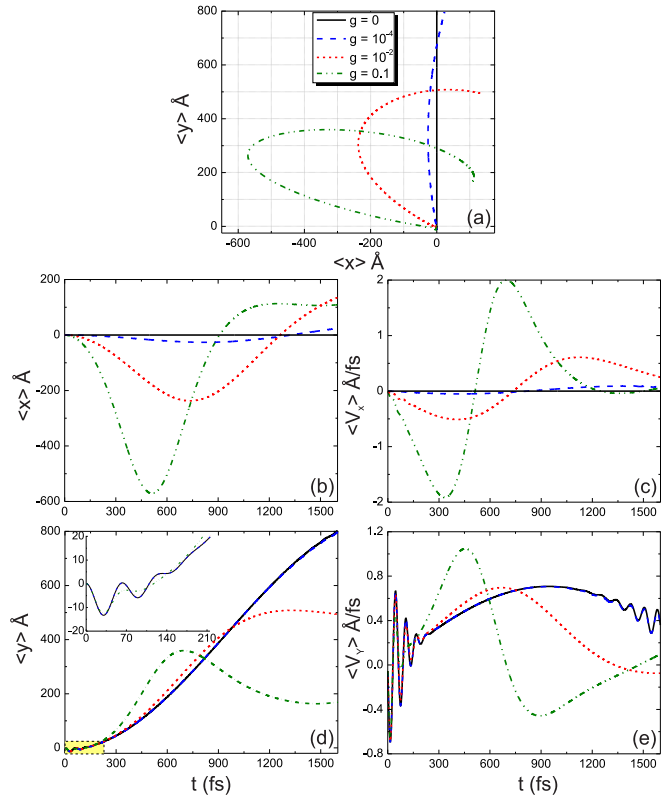

FIG. 5. (a) Trajectories drawn by $\langle x\rangle$ and $\langle y\rangle$ within $t = 1600$ fs propagation time. (b) and (d) Average positions and (c) and (e) expectation values of the velocities in the x and y directions, respectively, as a function of time for a Gaussian wave packet with initial pseudospin polarization $[c_1, c_2]^T = [1, 0]^T$, width $d = l_B = 81.13$ Å, and initial momentum $k_x = 0.035$ Å^{-1}. The results are obtained for different metrics: $g = 0$ (solid black lines), $g = 10^{-4}$ (dashed blue lines), $g = 10^{-2}$ (red dotted lines), and $g = 0.1$ (green dash-dotted lines). The inset in (d) is an enlargement of the first time steps.

In order to exemplify the effect of the metric in the wave packet dynamics, we shall discuss next the results for the two Gaussian distributions along the sublattices considered most in the study of wave packet propagation: $[c_1, c_2]^T = [1, 0]^T$ (Sec. III A) and $[c_1, c_2]^T = [1, 1]^T$ (Sec. III A). Since such analysis for undeformed monolayer graphene was reported in detail in Refs. [14,62,74], here we focus mainly on the differences that arises due to the different metric.

A. $[c_1, c_2]^T = [1, 0]^T$

We first consider the simple case where the lower component of the initial electronic wave function is zero, i.e., taking $c_1 = 1$ and $c_2 = 0$. This corresponds to the situation in which the electron probability is initially located only at the A sublattice of the graphene monolayer.

The trajectory drawn by $\vec{r(t)} = (\langle x(t)\rangle, \langle y(t)\rangle)$ for such a packet in the xy plane after a $t = 1600$ fs propagation time is shown in Fig. 5(a). As expected due to the effect of an external perpendicular magnetic field, the charge carrier travels in a cyclotron orbit, and moreover, by assuming a non-null g parameter, the radii of these orbits are strongly

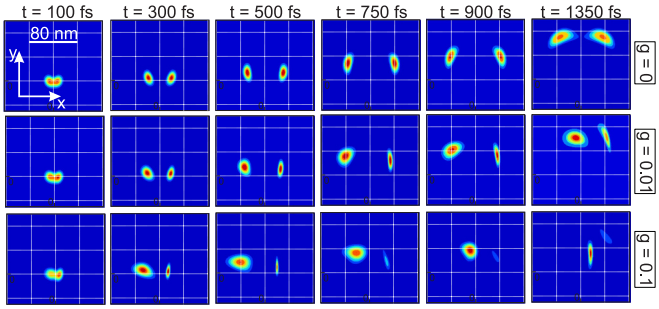

FIG. 6. Time evolution of electronic wave packet for the case $[c_1, c_2]^T = [1, 0]^T$ for the same parameters as in Fig. 5 at the time steps, from left to right, $t = 100$ fs, $t = 300$ fs, $t = 500$ fs, $t = 750$ fs, $t = 900$ fs, and $t = 1350$ fs and assuming the metric is $g = 0$ (top), $g = 0.01$ (middle), and $g = 0.1$ (bottom). The wave packet starts at $(x_0, y_0) = (0, 0)$ Å.

affected, as we shall discuss below. The expectation values of position and velocity as a function of time for different metrics are depicted in Figs. 5(b) and 5(d) and 5(c) and 5(e), respectively. Results for metrics $g = 0$, $g = 10^{-4}$, $g = 10^{-2}$, and $g = 0.1$ are shown by solid black lines, dashed blue lines, dotted red lines, and green dash-dotted lines, respectively. We can see that the average values of position and velocity in the x direction remain constant for the undeformed graphene case ($g = 0$). However, when a non-null g is considered, the average position and velocity in the x direction are no longer zero and exhibit variations with the time evolution that are more evident the greater the metric amplitude is. This can be easily understood by keeping in mind that the introduction of a different metric induces a renormalization of the Fermi velocity, as discussed in Sec. II, leading to a non-null value for $\langle v_x \rangle$. Moreover, this behavior will be clarified next when we discuss the symmetries of the total probability density for different time steps. On the other hand, by analyzing the average values of position and velocity in the y direction, one observes a clear oscillation even for $g = 0$, as emphasized in the inset of Fig. 5(d), in the first time steps of the wave packet evolution that are damped as time evolves. This oscillatory behavior indicates the manifestation of the Zitterbewegung effect along the y direction, as already reported [14,19,62,74] in the literature for this pseudospin configuration for the undeformed graphene case and confirmed here for $g = 0$ [see the black line in Fig. 5(d)]. Moreover, one notices that such oscillations exhibit a transient character, disappearing after a few hundred femtoseconds, and that the duration time and amplitude of the transient Zitterbewegung for $\langle y \rangle$ decay faster as the metric value increases.

For a better understanding of the average position and velocity behaviors in the x and y directions of Fig. 5, we analyze the contour plots of the squared modulus $|\Psi|^2$ of the propagated wave functions at different time steps. The results are depicted in Fig. 6 for cases $g = 0$ (upper panels), $g = 0.01$ (middle panels), and $g = 0.1$ (bottom panels) and for the following time steps: from left to right, $t = 100$ fs, $t = 300$ fs, $t = 500$ fs, $t = 750$ fs, $t = 900$ fs, and $t = 1350$ fs. Note that as the time evolves, the Gaussian wave packet, which starts with a circularly symmetric shape, splits into two parts moving with opposite velocities along the x axis. This splitting leads to vanishing oscillations in the average position and expectation values of velocity along the y direction [see Figs. 5(d) and 5(e)] after $t \approx 180$ fs, which explains the transient behavior of the Zitterbewegung. The trajectory of the wave packet is described by a circular cyclotron orbit, which is clearly visible in Fig. 5(a) and also evident in Fig. 6 from the fact that the wave packet bends for large time steps (see the last columns in Fig. 6) and by the average position of the y coordinate, which has an extra oscillation with a large amplitude associated with the radius of the cyclotron orbit. Therefore, from Figs. 5 and 6 one can see that the higher the amplitude of the g parameter is, the smaller the radius of the cyclotron orbit is. For the undeformed graphene case (top panels for $g = 0$), the two propagating subpackets move symmetrically with respect to $x = 0$, i.e., $|\Psi(x, y, t)|^2 = |\Psi(-x, y, t)|^2$ for a fixed time step. In contrast, for the non-null g case (see the middle and bottom panels for $g = 0.01$ and $g = 0.1$) the portions of probability amplitudes and widths of the two subpackets are noticeably different, and they are increasingly distorted into an elliptic shape at higher g values. This strong asymmetry in the total probability density is due to the assumed position-dependent spatial metric that, in turn, can be linked with strong anisotropy in the Fermi velocity and linear momentum to the electron motion, such that the momentum contributions along the negative and positive x directions are different and thus give rise to two propagating subpackets asymmetric with respect to each other, with one of them being more elliptical. Moreover, it is interesting to note that this large asymmetry in the probability density explains the less evident Zitterbewegung effect and the reduction of the transient time and is related to the reason why one gets a non-null average position for the x coordinate. Note that since the probability densities of the two subpackages for $g \neq 0$ are not the same, the contributions to the total average position value of the center of mass will be different, causing changes in the trajectories and average values of position and velocity, as shown in Fig. 5.

B. $[c_1, c_2]^T = [1, 1]^T$

We now investigate the case in which the wave function is equally distributed in sublattices A and B, which is equivalent to choosing $c_1 = c_2 = 1$. Like in the previous case (Sec. III A), we analyze the time evolution of average values of position and velocity along the x and y directions, the trajectories evolved in time, and the snapshots of the total probability density at different time steps, with the results displayed in Figs. 7 and 8, respectively, for the same parameters assumed in Sec. III A.

The trajectories drawn by $\vec{r(t)} = (\langle x(t) \rangle, \langle y(t) \rangle)$ and the expectation values of the position and velocities along the two x and y coordinates shown in Fig. 7 are non-null for $t > 0$ and do not remain constant as a function of time even for the undeformed graphene case (compare Fig. 7 with Fig. 5), unlike the previous case for $[1, 0]^T$. Note from Figs. 7(d) and 7(e) that the average values of position and velocity along the y direction exhibit less pronounced oscillations, as emphasized in the inset of Fig. 7(e). In order to understand the origin of this weak (or absent) oscillation in the average physical

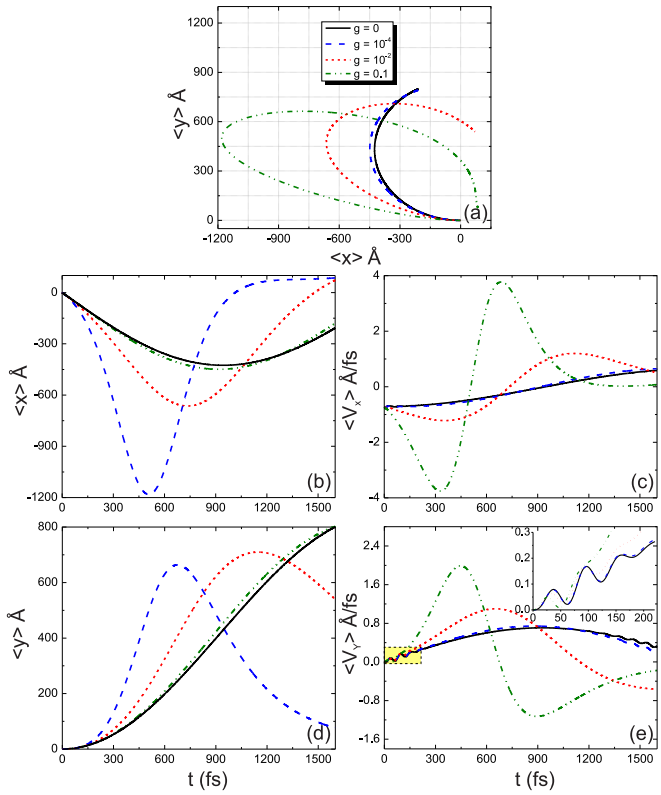

FIG. 7. The same as in Fig. 5, but now for a Gaussian wave packet with pseudospin polarization $[c_1, c_2]^T = [1, 1]^T$. The inset in (e) is an enlargement to emphasize the oscillatory behavior of $\langle v_y \rangle$ for the first time steps.

variables for this chosen pseudopsin polarization, we verify the spatial time evolution of the initial wave packet by showing snapshots for $t > 0$ of the total probability density in Fig. 8. Notice that regardless of the g value, the wave packet for this pseudospin configuration does not split into two subpackets as it does for the previous configuration (see Fig. 6), which is the reason why the electronic motion for this case does not exhibit Zitterbewegung. In the current case, the electronic trajectory is similar to the one for the left subpacket in Fig. 6, causing the packet width to deform and vary as time evolves due to the position-dependent spatial metric that works in a way similar to the position-dependent effective masses and anisotropic Fermi velocity. Also similar to the previous pseudospin case, here the trajectory of the Gaussian

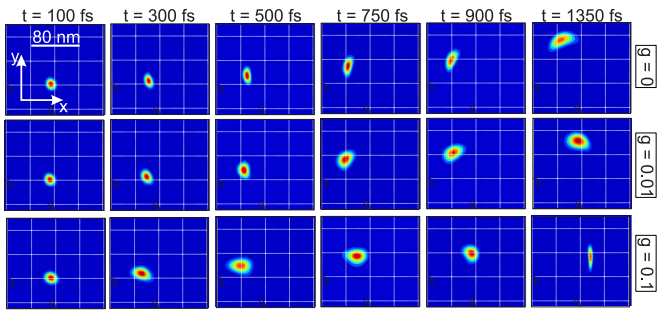

FIG. 8. The same as in Fig. 6, but now for a Gaussian wave packet with pseudospin polarization $[c_1, c_2]^T = [1, 1]^T$.

wave packet center of mass is given by a cyclotronic orbit that drastically changes when increasing the metric amplitude, leading to a deformed elliptic orbit that is more squeezed the greater the g parameter is [see Fig. 7(a)]. The oscillation in Fig. 7(d) for $\langle v_y \rangle$ is related to the asymmetric spreading over time of the wave packet.

IV. CONCLUSIONS

In summary, we have investigated the effects of metric changes in the electronic properties and in the time evolution of a low-energy two-dimensional Gaussian wave packet for graphene by means of the position-dependent translation operator formalism. We showed that such a formalism is able to introduce additional control of such properties and that the studied system mimics two different physical scenarios: a deformed graphene due to strain and a nonuniform mass term, induced by a specific substrate, that varies on a length scale much greater than the magnetic field length. A more direct analogy with the position-dependent spatial metric in this formalism is done with the first scenario when taking into account a unidirectional deformation that induces renormalized and position-dependent linear momentum and Fermi velocity.

With respect to the electronic properties, we analytically derived the Landau levels and their respective wave functions. An additional contribution term for the Landau levels was found with $\sqrt{g}$ dependence, and we showed that this term is responsible for performing a contraction of the levels; that is, the metric changes shift the Landau level to lower values and decrease the level spacing. The total wave function and the two pseudospin components are strongly affected by a non-null metric g, leading to a delocalization of the wave function.

By using the well-known split-operator technique and the deformed Dirac Hamiltonian in the presence of an external magnetic field developed in the position-dependent translation operator formalism, we investigated the wave packet dynamics for different metrics and for different choices of the initial pseudospin polarization. We analyzed the results for the expectation values of center-of-mass coordinates, the trajectories, the spreading of the wave packet in real space, and their oscillations due to Zitterbewegung. In general, we demonstrated that the non-null metric leads to asymmetry for the wave packet evolution, and therefore, in some cases it brings up oscillations in the average of the physical observables, and in other cases it suppresses the Zitterbewegung. The strong asymmetry in the total probability density is due to the position-dependent spatial metric that, in turn, can be linked to strong anisotropy in the Fermi velocity and linear momentum in the electron motion. We observed that the higher the amplitude of the g parameter is, the smaller the radius of the circular cyclotron orbit described by the electron is due to the presence of magnetic field and the more deformed it becomes.

The theoretical formalism used here could be useful for comparison and analogy to other two-dimensional-based systems, and we believe that the discussions of the results found in this work will contribute to a better understanding of the position-dependent translation operator formalism applied for two-dimensional materials.

ACKNOWLEDGMENTS

The authors are grateful to the National Counsel of Scientific and Technological Development (CNPq) and to the National Council for the Improvement of Higher Education (CAPES) of Brazil for financial support. R.N.C.F. is supported by CNPq Grant No. 312384/2018-1, and D.R.C. by Grants No. 310019/2018-4 and No. 437067/2018-1, respectively.

[1] K. S. Novoselov, A. K. Geim, S. V. Morozov, D. Jiang, Y. Zhang, S. V. Dubonos, I. V. Grigorieva, and A. A. Firsov, Science **306**, 666 (2004).
[2] A. H. Castro Neto, F. Guinea, N. M. R. Peres, K. S. Novoselov, and A. K. Geim, Rev. Mod. Phys. **81**, 109 (2009).
[3] R. S. Deacon, K.-C. Chuang, R. J. Nicholas, K. S. Novoselov, and A. K. Geim, Phys. Rev. B **76**, 081406(R) (2007).
[4] J. W. McClure, Phys. Rev. **104**, 666 (1956).
[5] M. Ramezani Masir, P. Vasilopoulos, A. Matulis, and F. M. Peeters, Phys. Rev. B **77**, 235443 (2008).
[6] L.-J. Yin, K.-K. Bai, W.-X. Wang, S.-Y. Li, Y. Zhang, and L. He, Front. Phys. **12**, 127208 (2017).
[7] W. Zawadzki and T. M. Rusin, J. Phys.: Condens. Matter **23**, 143201 (2011).
[8] W. Zawadzki, J. Phys.: Condens. Matter **29**, 373004 (2017).
[9] J. Schliemann, D. Loss, and R. M. Westervelt, Phys. Rev. Lett. **94**, 206801 (2005).
[10] J. Schliemann, D. Loss, and R. M. Westervelt, Phys. Rev. B **73**, 085323 (2006).
[11] V. Y. Demikhovskii, G. M. Maksimova, and E. V. Frolova, Phys. Rev. B **78**, 115401 (2008).
[12] W. Zawadzki, Phys. Rev. B **72**, 085217 (2005).
[13] M. I. Katsnelson, Eur. Phys. J. B **51**, 157 (2006).
[14] G. M. Maksimova, V. Y. Demikhovskii, and E. V. Frolova, Phys. Rev. B **78**, 235321 (2008).
[15] J. C. Martinez, M. B. A. Jalil, and S. G. Tan Martinez, Appl. Phys. Lett. **97**, 062111 (2010).
[16] R. Englman and T. Vértesi, Phys. Rev. B **78**, 205311 (2008).
[17] T. M. Rusin and W. Zawadzki, Phys. Rev. B **76**, 195439 (2007).
[18] T. M. Rusin and W. Zawadzki, Phys. Rev. B **80**, 045416 (2009).
[19] T. M. Rusin and W. Zawadzki, Phys. Rev. B **78**, 125419 (2008).
[20] J. Schliemann, New J. Phys. **10**, 043024 (2008).
[21] V. Krueckl and T. Kramer, New J. Phys. **11**, 093010 (2009).
[22] E. Romera and F. de los Santos, Phys. Rev. B **80**, 165416 (2009).
[23] Y. X. Wang, Z. Yang, and S. J. Xiong, Europhys. Lett. **89**, 17007 (2010).
[24] E. Romera, J. B. Roldán, and F. de los Santos, Phys. Lett. A **378**, 2582 (2014).
[25] A. Singh, T. Biswas, T. K. Ghosh, and A. Agarwal, Eur. Phys. J. B **87**, 275 (2014).
[26] S. M. Cunha, D. R. da Costa, G. O. de Sousa, A. Chaves, J. M. Pereira, and G. A. Farias, Phys. Rev. B **99**, 235424 (2019)
[27] S. Benczik, L. N. Chang, D. Minic, and T. Takeuchi, Phys. Rev. A **72**, 012104 (2005).
[28] P. Pedram, Phys. Rev. D **85**, 024016 (2012).
[29] P. Bosso, Phys. Rev. D **97**, 126010 (2018).
[30] M. Lubo, Phys. Rev. D **61**, 124009 (2000).
[31] F. Scardigli and R. Casadio, Eur. Phys. J. C **75**, 425 (2015).
[32] M. A. C. Rossi, T. Giani, and M. G. A. Paris, Phys. Rev. D **94**, 024014 (2016).
[33] Q. Zhao, M. Faizal, and Z. Zaz, Phys. Lett. B **770**, 564 (2017).
[34] L. B. Castro and A. E. Obispo, J. Phys. A **50**, 285202 (2017).
[35] M. Moniruzzaman and S. B. Faruque, J. Sci. Res. **10**, 99 (2018).
[36] B. Bolen and M. Cavaglià, Gen. Relativ. Gravitation **37**, 1255 (2005).
[37] S. Mignemi, Mod. Phys. Lett. A **25**, 1697 (2010).
[38] A. Kempf, J. Math. Phys. **35**, 4483 (1994).
[39] M. Ashgari, P. Pedram, and K. Nozari, Phys. Lett. B **725**, 451 (2013).
[40] R. N. Costa Filho, M. P. Almeida, G. A. Farias, and J. S. Andrade, Jr., Phys. Rev. A **84**, 050102(R) (2011).
[41] R. N. Costa Filho, J. P. M. Braga, J. H. S. Lira, and J. S. Andrade, Jr., Phys. Lett. B **755**, 367 (2016).
[42] J. P. M. Braga and R. N. Costa Filho, Int. J. Mod. Phys. C **27**, 1650047 (2016).
[43] R. N. Costa Filho, G. Alencar, B. S. Skagerstam, and J. S. Andrade, Europhys. Lett. **101**, 10009 (2013).
[44] F. S. A. Cavalcante, R. N. Costa Filho, J. Ribeiro Filho, C. A. S. de Almeida, and V. N. Freire, Phys. Rev. B **55**, 1326 (1997).
[45] M. A. Rego-Monteiro and F. D. Nobre, Phys. Rev. A **88**, 032105 (2013).
[46] M. Vubangsi, M. Tchoffo, and L. C. Fai, Phys. Scr. **89**, 025101 (2014).
[47] E. G. Barbagiovanni, D. J. Lockwood, N. L. Rowell, R. N. Costa Filho, I. Berbezier, G. Amiard, L. Favre, A. Ronda, M. Faustini, and D. Grosso, J. Appl. Phys. **115**, 044311 (2014).
[48] E. G. Barbagiovanni and R. N. C. Filho, Phys. E (Amsterdam, Neth.) **63**, 14 (2014).
[49] B. G. da Costa and E. P. Borges, J. Math. Phys. **55**, 062105 (2014).
[50] D. R. da Costa, A. Chaves, M. Zarenia, J. M. Pereira, Jr., G. A. Farias, and F. M. Peeters, Phys. Rev. B **89**, 075418 (2014).
[51] L. J. P. Xavier, D. R. da Costa, A. Chaves, J. M. Pereira, Jr., and G. A. Farias, J. Phys.: Condens. Matter **28**, 505501 (2016).
[52] Y. Aharonov and A. Casher, Phys. Rev. A **19**, 2461 (1979).
[53] Y. Betancur-Ocampo, M. E. Cifuentes-Quintal, G. Cordourier-Maruri, and R. de Coss, Ann. Phys. (NY) **359**, 243 (2015).
[54] F. M. D. Pellegrino, G. G. N. Angilella, and R. Pucci, Phys. Rev. B **84**, 195404 (2011).
[55] F. de Juan, M. Sturla, and M. A. H. Vozmediano, Phys. Rev. Lett. **108**, 227205 (2012).
[56] M. O. Goerbig, J. N. Fuchs, G. Montambaux, and F. Piéchon, Phys. Rev. B **78**, 045415 (2008).
[57] G. G. Naumis, S. Barraza-Lopez, M. Oliva-Leyva, and H. Terrones, Rep. Prog. Phys. **80**, 096501 (2017).
[58] P. Nigge, A. C. Qu, É. Lantagne-Hurtubise, E. Mårsell, S. Link, G. Tom, M. Zonno, M. Michiardi, M. Schneider, S. Zhdanovich, G. Levy, U. Starke, C. Gutiérrez, D. Bonn, S. A. Burke, M. Franz, and A. Damascelli, Sci. Adv. **5**, eaaw5593 (2019).
[59] M. O. Goerbig, Rev. Mod. Phys. **83**, 1193 (2011).
[60] S. Kuru, J. Negro, and L. M. Nieto, J. Phys.: Condens. Matter **21**, 455305 (2009).

[61] T. K. Ghosh, J. Phys.: Condens. Matter **21**, 045505 (2009).
[62] A. Chaves, L. Covaci, Kh. Yu. Rakhimov, G. A. Farias, and F. M. Peeters, Phys. Rev. B **82**, 205430 (2010).
[63] A. Chaves, G. A. Farias, F. M. Peeters, and R. Ferreira, Commun. Comput. Phys. **17**, 850 (2015).
[64] Kh. Yu. Rakhimov, A. Chaves, G. A. Farias, and F. M. Peeters, J. Phys.: Condens. Matter **23**, 275801 (2011).
[65] J. M. Pereira, Jr., F. M. Peeters, A. Chaves, and G. A. Farias, Semicond. Sci. Technol. **25**, 033002 (2010).
[66] M. H. Degani and M. Z. Maialle, J. Comput. Theor. Nanosci. **7**, 454 (2010).
[67] A. Chaves, G. A. Farias, F. M. Peeters, and B. Szafran, Phys. Rev. B **80**, 125331 (2009).
[68] D. R. da Costa, A. Chaves, S. H. R. Sena, G. A. Farias, and F. M. Peeters, Phys. Rev. B **92**, 045417 (2015).
[69] D. R. da Costa, A. Chaves, G. A. Farias, L. Covaci, and F. M. Peeters, Phys. Rev. B **86**, 115434 (2012).
[70] L. S. Cavalcante, A. Chaves, D. R. da Costa, G. A. Farias, and F. M. Peeters, Phys. Rev. B **94**, 075432 (2016).
[71] A. Chaves, D. R. da Costa, G. O. de Sousa, J. M. Pereira, Jr., and G. A. Farias, Phys. Rev. B **92**, 125441 (2015).
[72] D. R. da Costa, A. Chaves, G. A. Farias, and F. M. Peeters, J. Phys.: Condens. Matter **29**, 215502 (2017).
[73] H. M. Abdullah, D. R. da Costa, H. Bahlouli, A. Chaves, F. M. Peeters, and B. Van Duppen, Phys. Rev. B **100**, 045137 (2019).
[74] I. R. Lavor, D. R. da Costa, A. Chaves, S. H. R. de Sena, G. de A. Farias, B. Van Duppen, and F. M. Peeters, J. Phys.: Condensed Matter (2020), doi:10.1088/1361-648X/abcd7f.
[75] S. M. Cunha, D. R. da Costa, L. C. Felix, A. Chaves, and J. M. Pereira, Jr., Phys. Rev. B **102**, 045427 (2020).